



Contents lists available at ScienceDirect

Journal of Power Sources

journal homepage: www.elsevier.com/locate/jpowsour

Short communication

Self-assembly of disordered hard carbon/graphene hybrid for sodium-ion batteries



Linghong Yin^a, Yixian Wang^a, Congcong Han^a, Yong-Mook Kang^b, Xiao Ma^a, Hui Xie^a, Mingbo Wu^{a,*}

^a State Key Laboratory of Heavy Oil Processing, College of Chemical Engineering, China University of Petroleum, Qingdao 266580, China

^b Department of Energy and Materials Engineering, Dongguk University-Seoul, Seoul, 100-715, South Korea

HIGHLIGHTS

- Disordered hard carbon/graphene hybrid was successfully prepared.
- Unique structure with carbon layers and numerous microspheres growing on graphene.
- High capacity and rate capability as anode material for SIBs.

ARTICLE INFO

Article history:

Received 22 July 2015

Received in revised form

4 November 2015

Accepted 20 November 2015

Available online xxx

Keywords:

Disordered hard carbon

Graphene

Anode

Sodium-ion batteries

ABSTRACT

Disordered hard carbon/graphene (C@G) hybrid is successfully designed and prepared for the first time through a facile route. SEM and TEM analyses show the uniform distribution of carbon microspheres and carbon layers on the surface of graphene. As an anode material of sodium-ion batteries, such a construction could ensure an effective contact area with the electrolyte and offer massive active sites. It displays a stable sodium storage capacity of $\sim 300 \text{ mAh g}^{-1}$ after 100 cycles at a current density of 50 mA g^{-1} and exhibits an excellent rate performance. The unique structure and advantageous synergistic effect between disordered hard carbon and graphene make a significant contribution to the good Na^+ insertion/extraction property.

© 2015 Elsevier B.V. All rights reserved.

1. Introduction

Lithium-ion batteries (LIBs) are important energy storage devices with high energy density, long cycle life and environmental benignity [1–3]. Although LIBs have been prosperous in portable electronics, they face many challenges such as high cost and limited lithium source. Advanced energy storage devices are urgently needed to satisfy the continuously increasing demand. Sodium-ion batteries (SIBs) are one of the promising candidates as power source and possible substitute of LIBs [4,5]. Recently, SIBs have drawn much attention due to their similar electrochemical mechanism, comparatively low cost and abundant sodium source [6].

However, suitable anode materials with higher sodium storage capacity, longer cyclic and faster charge–discharge rate

performance still remain challenging [7]. The typical graphite as dominant commercial anode material of LIBs shows poor electrochemical performance in SIBs because of the larger ionic diameter of sodium [8]. Lots of attempts have been made to explore suitable anode materials to meet the demand of energy storage equipment [9,10]. Among those candidates, hard carbon materials with low degree of graphitization and larger interlayer space hold good prospect. To date, diverse carbon nanostructures from different precursors (including biomass and polymers) have been designed successfully, e.g. nanofibers [11], nanosheets [12], hollow nanospheres [13]. These works have demonstrated that hard carbon materials with attractive morphology could improve the electrochemical performance. Graphene with excellent electronic conductivity and thermal stability has been paid widely attention. As an anode material of SIBs, it ensures good electronic transmission channel and structural stability [14]. Moreover, the structure with two-dimensional thin layers can not only shorten Na^+ diffusion path, but also possess higher sodium storage potential. Therefore,

* Corresponding author.

E-mail address: wumb@upc.edu.cn (M. Wu).

disordered hard carbon/graphene hybrid with unique morphology could be a reasonable design to further enhance the electrochemical performance of anode material for SIBs.

In this article, we construct a novel disordered hard carbon/graphene (C@G) hybrid by in situ synthesizing graphene-like carbides with abundant carbon microspheres on the surface. The unique structure can accelerate mass transport effectively by providing a large contact area with the electrolyte and a short Na⁺ diffusion path. As a consequence, the obtained C@G exhibits a stable reversible capacity and an excellent rate performance.

2. Experimental

All chemicals were of analytical grade and used directly without further purification. In a typical process, graphite oxide was synthesized by a modified Hummers' method [15]. Briefly, 5 g sucrose and 225 mg graphite oxide were dissolved in 75 mL deionized water followed by sonication for 3 h. The obtained suspension was transferred to a 100 mL Teflon-sealed autoclave and maintained at 190 °C for 12 h. After cooling down to room temperature, the resultant product was washed with deionized water and dried in a vacuum at 60 °C. Finally, C@G hybrid was obtained after calcining at 700 °C for 2 h in N₂ atmosphere. For comparison, pure carbon powder (CP) without adding graphite oxide and pure graphene (GN) without adding sucrose were synthesized by the same method as mentioned above.

The morphologies of obtained samples were investigated using field emission scanning electron microscopy (SEM, Hitachi S-4800, Japan), transmission electron microscopy (TEM, JEM-2100UHR, Japan). X-ray diffraction (XRD) analysis was recorded on X'Pert PRO MPD (Holland) with Cu K α radiation. Raman analysis was performed on a Jobin Yvon HR800 Raman spectrometer. Nitrogen adsorption–desorption isotherms were carried out on ASAP 2020 Micromeritics instrument. X-ray photoelectron spectroscopy (XPS) was performed on Thermo ESCALAB 250XI with a monochromatic Al K X-ray source.

The sodium coin cells were assembled in an argon-filled glove box by using pure sodium foil as the counter and reference electrode. The electrolyte was 1 M NaClO₄ in ethylene (EC) and diethyl carbonate (DEC) (v:v = 1:1). The working electrodes were prepared by pasting the slurry of the active materials (80 wt.%), carbon black (10 wt.%) and poly(vinylidene) fluoride (10 wt.%) in N-methyl-2-pyrrolidinone on Cu foils. Then dried at 100 °C in a vacuum for 10 h. Galvanostatic charge–discharge measurements were performed on a Land CT2001A cycler. Cyclic voltammetry (CV) tests were carried out on a CHI660D Electrochemistry Workstation at a scan rate of 0.1 mV s⁻¹ between 0.01 and 3 V. Electrochemical impedance spectroscopy (EIS) studies (signal amplitude, 10 mV; frequency range, 0.01–100000 Hz) were measured on Ametek PARSTAT4000 electrochemistry workstation.

3. Results and discussion

The detailed surface morphologies and microstructure of as-obtained samples were studied by SEM and TEM. Fig. S1A displays SEM image of GN. Flexible graphene sheets and some obvious corner angles on the surface can be found. From SEM image of CP (Fig. S1B), numerous carbon microspheres inherit an interconnected structure, which is consistent with the reported literature [16]. As shown in Fig. 1A, abundant carbon microspheres grow uniformly on elastic graphene skeleton, as seeds germinate in the field and then sprout out to grow into carbon microspheres. No separated carbon microspheres are observed, suggesting carbon microspheres around 450 nm are attached on graphene framework.

TEM image of GN (Fig. S2) shows typical thin film-like structure

with transparent surface and numerous wrinkles which reflect the corner angles have been observed in Fig. S1A. Fig. 1B depicts TEM image of C@G, the surface of graphene sheets are coated with carbon layers and the wrinkles exhibit nanotubular structure around 45.8 nm of diameter. The green arrows are corner angles of graphene, while the yellow arrows correspond to carbon layers. The TEM image also reveals the clear outline of carbon microspheres. Through SEM and TEM observations, it can be concluded that carbon microspheres were grown on the surface of carbon layers which distributed uniformly on the graphene sheets.

The XRD pattern of the as-prepared C@G is illustrated in Fig. 2A. As can be seen, it presents two broad, weak diffraction peaks corresponding to the (002) and (100) diffraction modes at about 23.7° and 43.4°, characteristic of a disordered carbonaceous structure. The interlayer spacing (d_{002}) is calculated to be ~0.375 nm, which is obviously larger than that of graphite (0.335 nm). It is worth noting that the large interlayer distance would facilitate the reversible Na⁺ storage and transport [13]. Raman spectroscopy was employed to investigate the graphitization degree of C@G. As displayed in Fig. 2B, it confirms the presence of D band (1341 cm⁻¹) and G band (~1587 cm⁻¹) of amorphous carbon. D band results from disorder, structural defects and associates with the formation of sp³ defect bonds [17]. G band corresponds to the structural integrity of graphite. The intensity ratio (I_D/I_G) of C@G is 0.934, higher than 0.773 of CP, indicating abundant defects and evident disordered carbonaceous structure in C@G. The presence of defects could favor Na⁺ diffusion [18] and provide more adsorption sites by increasing charge transfer between adatoms and defects [19].

The specific surface area and pore structure of GN and C@G hybrid were further characterized by nitrogen adsorption–desorption isotherms. GN exhibits major pore size distributions in the meso- and macroranges with a BET surface area of 399 m² g⁻¹ and an average pore size of 14.4 nm (Fig. S3). C@G hybrid displays a larger BET surface area of 488 m² g⁻¹ and mainly possesses micropores with an average pore diameter of 1.6 nm (Fig. 2C). The highly dispersed carbon microspheres and carbon layers on the surface of graphene contribute to the increase in the surface area and decrease in the mean pore size compared with that of pure GN. The pore structure agrees well with that of sucrose-derived hard carbon reported previously [20]. The high surface area could offer a large electrode/electrolyte contact area and provide Na⁺ with more active sites [13,21], while porosity largely influences the Na⁺ adsorption ability, especially micropores according to the mechanism for sodium insertion [22].

The full-range XPS spectrum of C@G in Fig. S4 shows a significant XPS C1s peak at about 285 eV (97.02 at%), along with a much weaker O1s peak at about 534 eV (2.98 at%), indicating only a few oxygen-containing functional groups exist. The C1s XPS spectra (Fig. 2D) analysis indicates that the strongest peak of sp² carbon appears at a binding energy of 284.6 eV. In addition, there are other weaker peaks such as sp³-bonded carbon (285.4 eV), C–O (286.6 eV) and C=O (288.5 eV) [23]. The low content of C=O indicates that most carboxyl and hydroxyl functional groups were reduced [24]. The existence of a few oxygen-containing groups could enhance the sodium uptake [25,26] and contribute to Na storage [27] though it may lead to initial irreversible Coulombic efficiency [24].

The electrochemical behavior of C@G as anode material of SIBs was investigated by CV and galvanostatic charge–discharge measurements. Fig. 3A displays CV curves of C@G electrode for the first three cycles from 0.01 to 3 V at a scanning rate of 0.1 mV s⁻¹. In the first CV scan, noticeable cathodic peaks are observed at 1.02 V, 0.42 V and near 0.02 V. The small peak at 1.02 V is ascribed to the reaction of sodium with functional groups at the electrode surface [13]. The large irreversible reduction peak at 0.42 V is attributed to

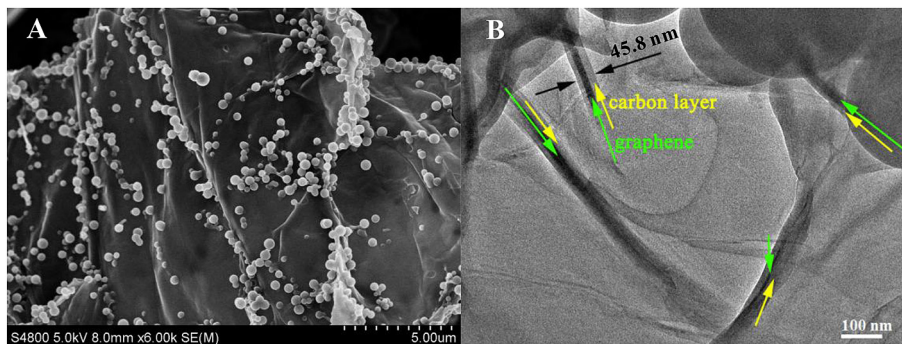


Fig. 1. (A) SEM and (B) TEM images of C@G.

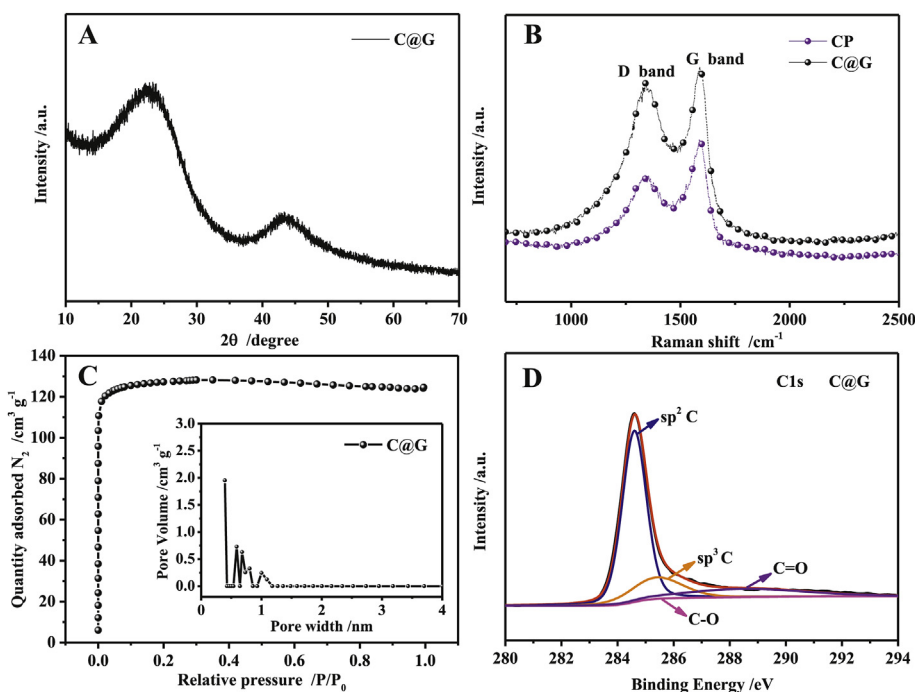


Fig. 2. (A) XRD pattern of C@G. (B) Raman spectra of CP and C@G. (C) Nitrogen adsorption–desorption isotherms and pore-size distribution of C@G. (D) XPS spectra of C1s region of C@G.

the decomposition of electrolyte, and the formation of a solid electrolyte interphase (SEI) layer [11]. The two peaks disappeared during the later cycles which are responsible for major irreversible specific capacity. Additionally, the clear cathodic peak at 0.02 V and anodic peak at 0.1 V are related to the reversible insertion/extraction of sodium in the hybrid and similar for lithium insertion/extraction in carbonaceous materials [28]. A pair of redox peaks occurring around 0.6 V in subsequent cycles mainly originate from the charge transfer on the surface of small graphitic crystallites [29,30]. The tiny changes of CV curve from the second cycle indicate a steady Na^+ insertion/extraction, which could react with C@G reversibly and leading to a good cycling performance.

The electrochemical performances of as-made C@G, CP and GN were evaluated by galvanostatic charge/discharge measurements between 0.01 V and 3 V at a current density of 50 mA g^{-1} . Fig. 3B shows the charge/discharge profile of C@G. During the first cycle, C@G electrode delivers an initial discharge/charge specific capacity of $807/355 \text{ mAh g}^{-1}$, corresponding to Coulombic efficiency of $\sim 44\%$. The large irreversible capacity in the voltage range of 0.9–0.2 V arises from the decomposition of electrolyte and the formation of

SEI layer. In the second cycle, the reversible discharge capacity is as high as 363 mAh g^{-1} , and the Coulombic efficiency goes up to 93 %, which indicates the highly reversible insertion/extraction of Na^+ into disordered graphite layers in C@G. A comparison of the charge/discharge cyclic performance and Coulombic efficiencies for C@G, CP, and GN is shown in Fig. 3C. As can be seen, GN and CP electrodes exhibit the initial discharge/charge capacities of $759/209$, $509/211 \text{ mAh g}^{-1}$ with initial Coulombic efficiencies of 27 and 41 %, respectively. The Coulombic efficiencies of all electrodes increase dramatically upon cycling and exhibit a much higher average Coulombic efficiency after 100 cycles. However, GN electrode still shows a much lower average Coulombic efficiency than that of C@G as a whole. The high Coulombic efficiency of C@G may be related to the excellent reversibility of Na^+ insertion into turbostratic disordered graphite layers and adsorption within the micropores [22]. C@G electrode also delivers a higher sodium storage capacity and the discharge capacity still remains 296 mAh g^{-1} even after 100 cycles, larger than that of GN (95 mAh g^{-1}) and CP (174 mAh g^{-1}). The enhanced sodium storage capacity and cycling stability of C@G can be ascribed to the synergistic effect of disordered hard carbon

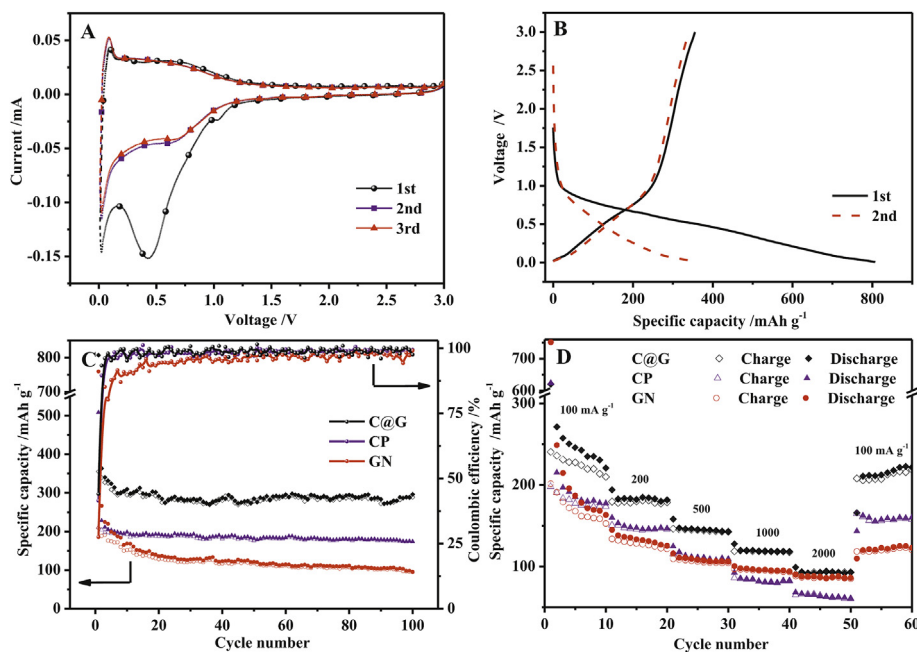


Fig. 3. (A) Cyclic voltammograms of C@G electrode at a scan rate of 0.1 mV s^{-1} between 0.01 and 3 V. (B) Voltage–capacity profile of C@G electrode at the current density of 50 mA g^{-1} . (C) Cycle performance and Coulombic efficiencies of C@G, CP and GN electrodes at the current density of 50 mA g^{-1} . (D) Rate performance of C@G, CP and GN electrodes at variant current densities.

and graphene that buffers the mechanical stress during Na^+ insertion/extraction process.

Fig. 3D shows the rate capabilities of C@G, CP and GN. C@G electrode delivers reversible capacities of 220, 181, 143, 118, 92 mAh g^{-1} at current densities of 100, 200, 500, 1000, 2000 mA g^{-1} , respectively. The remarkable rate performance of C@G should benefit from the large interlayer space that facilitates electron transfer and allows for the rapid access of Na^+ into bulk material. As the current density returns to 100 mA g^{-1} , the discharge capacity can recover to 222 mAh g^{-1} , higher than 160 and 123 mAh g^{-1} of CP and GN. From another perspective, such results also demonstrate the robustness of porous C@G networks, which can accommodate sodiation-induced stress and hold the superior reversibility [29,31]. To the best of our knowledge, the electrochemical performance of C@G in terms of cycling stability and rate capability are comparable to most of ever reported carbonaceous materials [11–14]. EIS measurements were applied to explore the effect of graphene on the interfacial impedance of C@G hybrid. Fig. S5 shows Nyquist plots of CP and C@G electrodes before cycling and after 50 cycles. The semicircle shows that interfacial impedance become smaller with the introduction of graphene. After 50 cycles, the resistance increase for C@G electrode is much lower than that of CP electrode, implying that the addition of graphene affectively reduces the interfacial impedance and facilitates the fast charge transport between the electrode and electrolyte. As a consequence, the two-dimensional graphene can effectively enhance the electrical conductivity of disordered hard carbon and endow a good electrochemical performance.

The enhanced cycling stability and rate capability of C@G electrode in SIBs could be attributed to the three reasons as follows: First of all, disordered hard carbon with different morphological characteristics (carbon layers and carbon microspheres) growing uniformly on graphene skeleton can ensure a sufficient contact area with electrolyte and minimize the volume variation. Secondly, the formation of carbon microspheres and thin thickness of carbon layers can offer massive active sites and guarantee a short Na^+

diffusion distance to some extent. Thirdly, the large interlayer space and numerous micropores would facilitate the reversible Na^+ storage and transport. Hence, the well-defined structure of C@G leads to a superior electrochemical performance as anode material of SIBs.

4. Conclusion

In summary, disordered hard carbon/graphene with unique morphology was successfully prepared by simple hydrothermal process and subsequent heat treatment. The well-defined structure of C@G with abundant carbon microspheres and carbon layers growing on graphene skeleton endowed a high sodium storage capacity, cyclic stability and rate performance. The good electrochemical performance proved that C@G could be a promising candidate for anode materials of SIBs. Furthermore, C@G with novel structure has great potential as functional materials for catalysts or other fields.

Acknowledgments

This work was supported by the National Natural Science Foundation of China (Grant No. 51172285, 51372277); The Fundamental Research Funds for the Central Universities (No.15CX08005A).

Appendix A. Supplementary data

Supplementary data related to this article can be found at <http://dx.doi.org/10.1016/j.jpowsour.2015.11.076>.

References

- [1] M. Armand, J.M. Tarascon, Building better batteries, *Nature* 451 (2008) 652–657.
- [2] S.H. Liu, Y.F. Dong, C.T. Zhao, Z.B. Zhao, C. Yu, Z.Y. Wang, J.S. Qiu, Nitrogen-rich carbon coupled multifunctional metal oxide/graphene nanohybrids for long-

- life lithium storage and efficient oxygen reduction, *Nano Energy* 12 (2015) 578–587.
- [3] Z.T. Li, G.L. Wu, D. Liu, W.T. Wu, B. Jiang, J.T. Zheng, Y.P. Li, J.H. Li, M.B. Wu, Graphene enhanced carbon-coated tin dioxide nanoparticles for lithium-ion secondary batteries, *J. Mater. Chem. A* 2 (2014) 7471–7477.
- [4] S.Y. Hong, Y. Kim, Y. Park, A. Choi, N.S. Choi, K.T. Lee, Charge carriers in rechargeable batteries: Na ions vs. Li ions, *Energy Environ. Sci.* 6 (2013) 2067–2081.
- [5] V. Palomares, P. Serras, I. Villaluenga, K.B. Hueso, J. Carretero-Gonzalez, T. Rojo, Na-ion batteries, recent advances and present challenges to become low cost energy storage systems, *Energy Environ. Sci.* 5 (2012) 5884–5901.
- [6] H.L. Pan, Y.S. Hu, L.Q. Chen, Room-temperature stationary sodium-ion batteries for large-scale electric energy storage, *Energy Environ. Sci.* 6 (2013) 2338–2360.
- [7] D.A. Stevens, J.R. Dahn, High capacity anode materials for rechargeable Sodium-ion batteries, *J. Electrochem. Soc.* 147 (2000) 1271–1273.
- [8] P. Ge, M. Foulletier, Electrochemical intercalation of sodium in graphite, *Solid State Ionics* 28–30 (1988) 1172–1175.
- [9] M. Dahbi, N. Yabuuchi, K. Kubota, K. Tokiwa, S. Komaba, Negative electrodes for Na-ion batteries, *Phys. Chem. Chem. Phys.* 16 (2014) 15007–15028.
- [10] Z.Q. Zhu, F.Y. Cheng, Z. Hu, Z.Q. Niu, J. Chen, Highly stable and ultrafast electrode reaction of graphite for sodium ion batteries, *J. Power Sources* 293 (2015) 626–634.
- [11] W. Luo, J. Schardt, C. Bommier, B. Wang, J. Razink, J. Simonsen, X.L. Ji, Carbon nanofibers derived from cellulose nanofibers as a long-life anode material for rechargeable sodium-ion batteries, *J. Mater. Chem. A* 1 (2013) 10662–10666.
- [12] J. Ding, H. Wang, Z. Li, A. Kohandehghan, K. Cui, Z. Xu, B. Zahiri, X. Tan, E.M. Lotfabad, B.C. Olsen, D. Mitlin, Carbon nanosheet frameworks derived from peat moss as high performance sodium ion battery anodes, *ACS Nano* 7 (2013) 11004–11015.
- [13] K. Tang, L.J. Fu, R.J. White, L.H. Yu, M.M. Titirici, M. Antonietti, J. Maier, Hollow carbon nanospheres with superior rate capability for sodium-based batteries, *Adv. Energy Mater.* 2 (2012) 873–877.
- [14] X.F. Luo, C.H. Yang, Y.Y. Peng, N.W. Pu, M.D. Ger, C.T. Hsieh, J.K. Chang, Graphene nanosheets, carbon nanotubes, graphite, and activated carbon as anode materials for sodium-ion batteries, *J. Mater. Chem. A* 3 (2015) 10320–10326.
- [15] W.S. Hummers, R.E. Offeman, Preparation of graphitic oxide, *J. Am. Chem. Soc.* 80 (1958) 1339.
- [16] A. Kurniawan, C. Effendi, L.K. Ong, F. Kurniawan, C.X. Lin, A.E. Angkawijaya, Y. Ju, S. Ismadji, X.S. Zhao, Preparation of nanoporous carbon microspheres by subcritical water carbonization and electrocapacitive study, *Electrochim. Acta* 111 (2013) 99–107.
- [17] O. Akhavan, E. Ghaderi, S. Aghayee, Y. Fereydooni, A. Talebi, The use of a glucose-reduced graphene oxide suspension for photothermal cancer therapy, *J. Mater. Chem.* 22 (2012) 13773–13781.
- [18] Y. C. Liu, N. Zhang, L. F. Jiao, J. Chen, Tin nanodots encapsulated in porous nitrogen-doped carbon nanofibers as a free-standing anode for advanced sodium-ion batteries, *Adv. Mater.* DOI: 10.1002/adma.201503015.
- [19] D. Datta, J.W. Li, V.B. Shenoy, Defective graphene as a high-capacity anode material for Na- and Ca-ion batteries, *ACS Appl. Mater. Interfaces* 6 (2014) 1788–1795.
- [20] T.Q. Chen, L.K. Pan, T. Lu, C.L. Fu, D.H.C. Chua, Z. Sun, Fast synthesis of carbon microspheres via a microwave-assisted reaction for sodium ion batteries, *J. Mater. Chem. A* 2 (2014) 1263–1267.
- [21] Y. Yan, Y.X. Yin, Y.G. Guo, L.J. Wan, A sandwich-like hierarchically porous carbon/graphene composite as a high-performance anode material for sodium-ion batteries, *Adv. Energy Mater.* 4 (2014) 1301584.
- [22] E. Irisarri, A. Ponrouch, M.R. Palacin, Review-Hard carbon negative electrode materials for sodium-ion batteries, *J. Electrochem. Soc.* 162 (2015) A2476–A2482.
- [23] L. Zhang, F. Zhang, X. Yang, G.K. Long, Y.P. Wu, T.F. Zhang, K. Leng, Y. Huang, Y.F. Ma, A. Yu, Y.S. Chen, Porous 3D graphene-based bulk materials with exceptional high surface area and excellent conductivity for supercapacitors, *Sci. Rep.* 3 (2013) 1408.
- [24] Y.X. Wang, S.L. Chou, H.K. Liu, S.X. Dou, Reduced graphene oxide with superior cycling stability and rate capability for sodium storage, *Carbon* 57 (2013) 202–208.
- [25] R. Alcántara, J.M. Jiménez-Mateos, P. Lavela, J.L. Tirado, Carbon black: a promising electrode material for sodium-ion batteries, *Electrochem. Commun.* 3 (2001) 639–642.
- [26] D. Billauda, L. Thevenot, P. Willmann, New electrochemical and chemical routes for the synthesis of lithium rich graphite intercalation compounds, *Electrochim. Acta* 45 (1999) 59–66.
- [27] K.L. Hong, L. Qie, R. Zeng, Z.Q. Yi, W. Zhang, D. Wang, W. Yin, C. Wu, Q.J. Fan, W.X. Zhang, Y.H. Huang, Biomass derived hard carbon used as a high performance anode material for sodium ion batteries, *J. Mater. Chem. A* 2 (2014) 12733–12738.
- [28] J.R. Dahn, T. Zheng, Y. Liu, J.S. Xue, Mechanisms for lithium insertion in carbonaceous materials, *Science* 270 (1995) 590–593.
- [29] X.S. Zhou, X.S. Zhu, X. Liu, Y. Xu, Y.X. Liu, Z.H. Dai, J.C. Bao, Ultralong cycle life sodium-ion battery anodes using a graphene-templated carbon hybrid, *J. Phys. Chem. C* 118 (2014) 22426–22431.
- [30] Y.L. Cao, L.F. Xiao, M.L. Sushko, W. Wang, B. Schwenzer, J. Xiao, Z.M. Nie, L.V. Saraf, Z.G. Yang, J. Liu, Sodium ion insertion in hollow carbon nanowires for battery applications, *Nano Lett.* 12 (2012) 3783–3787.
- [31] S. Komaba, W. Murata, T. Ishikawa, N. Yabuuchi, T. Ozeki, T. Nakayama, A. Ogata, K. Gotoh, K. Fujiwara, Electrochemical Na insertion and solid electrolyte interphase for hard-carbon electrodes and application to Na-ion batteries, *Adv. Funct. Mater.* 21 (2011) 3859–3867.